Proceedings of the 9th International Workshop on Ship and Marine Hydrodynamics, 26 – 28 August 2015, Glasgow, UK

Experimental study of the transitional flow of a sphere located at the free surface

Marion C. James*[1], Alex Forester[2], Dominic A. Hudson[1], Dominic J. Taunton[1], Stephen R. Turnock[1]

1. *Fluid-Structure Interactions Group, University of Southampton, Southampton SO16 7QF, UK*
2. *Computational Engineering and Design Group, University of Southampton, Southampton SO16 7QF, UK*

Abstract: The investigation of transitional flow past a sphere at the free surface is a challenging problem due to a complex interaction between the free surface and evolution of the boundary layer and resultant separation on the sphere's surface. An increased knowledge about the fluid phenomena around bluff bodies would be of benefit to the design of offshore structures and ships' bulbous bows. In this paper, experiments conducted in a towing tank environment are presented for a 225mm-diameter sphere towed at the free surface across the diameter based Reynolds number range $1.6 \times 10^5 < Re < 3.8 \times 10^5$. Measurements of the total resistance using a bespoke dynamometer are combined with above-water photographs to provide further insight. An abrupt change in flow regime was observed as speed increased to reach $Re \sim 3.5 \times 10^5$. The bow breaking wave grows until transition occurs into a smooth flow over the top of the sphere. This change in flow condition resulted in a 60% decrease in total resistance. This paper considers why this drag crisis phenomenon takes place around $Re \sim 2.6 - 3.6 \times 10^5$, which is similar to single-phase flows. The inertial effect of the free surface deformation as opposed to the influence of the laminar to turbulent boundary layer transition is investigated.

Keywords: Critical Reynolds number; turbulent flow; wave resistance; bluff bodies; free surface flow
Article ID: 1671-9433(2010)01-0000-00

1 Introduction

The flow past a sphere has been studied since the early 20th century in wind tunnels and water channels using both quantitative measurements and qualitative flow visualisation techniques. Research on the variation of the wake structure with diameter based Reynolds number indicates that below Reynolds number of 20, the flow is fully attached (Taneda, 1956).

When $Re \sim 24$, laminar flow separation occurs and stationary axi-symmetric rings are generated up to $Re \sim 210$ (Taneda (1956), Achenbach (1974a)). The vortex rings begin to oscillate around $Re \sim 270$ and horse-shoe shaped vortex loops are shed behind the sphere, leading to an unstable non-axi-symmetric wake (Achenbach, 1974a). The vortex loops diffuse rapidly and the wake flow becomes turbulent at $Re \sim 800$.

The turbulent region was studied by Achenbach (1972), who classified the different flow types observed into: sub-critical ($Re \leq 2 \times 10^5$), critical ($2 \times 10^5 \leq Re \leq 4 \times 10^5$), super-critical ($4 \times 10^5 \leq Re \leq 10^6$) and trans-critical ($Re \geq 10^6$). Using a surface oil flow visualisation technique, Taneda (1978) observed that the laminar boundary layer separates at an angle $\varphi_S = 80^o$ from the front stagnation point for $10^4 \leq Re \leq 3 \times 10^5$. Over the same experiment, Taneda (1978) used smoke to study the wake structure. At sub-critical Reynolds numbers, he characterised the near-wake as a large recirculating region with a progressive periodic motion of wave length $\lambda = 4.5D$ and velocity $\sim 0.9U$ and a constant Strouhal number of about 0.2, emphasising the strong periodicity of the rolled-up vortices. In addition, he observed an irregular rotation of the separation point. This random process was later explained by Kim and Durbin (1988), Sakamoto and Haniu (1990), Bakic and Peric (2005), Bakic et al. (2006) and Ozgoren et al. (2011). Indeed, besides the low-frequency mode of Strouhal number due to the large-scale instability of the turbulent wake behind the sphere, a co-existing high-frequency mode was identified due to periodic fluctuations of the shear layer.

As Reynolds number increases further ($Re \sim 3.5 \times 10^5$), Taneda (1978) observed a sudden change in the skin friction distribution on the downstream half of the sphere. The laminar boundary layer separation point moved to $\phi_S = 100^o$ on average. Moreover two other separation lines appeared further downstream indicating the presence of a separation bubble containing a vortex ring. The flow reattached at $\phi_S = 117^o$ (re-attachment line) and separated again at $\phi_S = 135^o$ (turbulent separation line). At the rear of the sphere, an Ω-shaped line was observed due to the reattachment of all the streamlines. Hair-pin vortices are shed at the rear of the sphere in an asymmetric manner (Kiya et al., 2000).

Quantitative measurements gathered by Hoerner (1965) and Achenbach (1972) have showed that the drag coefficient has a fairly constant value of 0.47 at sub-critical Reynolds numbers, but undergoes a sharp decrease down to 0.1 in the critical Reynolds number range. This phenomenon is well known under the name of 'drag crisis'. Due to the high turbulent mixing, the turbulent boundary layer has a higher momentum near the wall and is therefore better able to withstand the adverse pressure gradient at the rear of the sphere. Hence, the separated region gets smaller with higher pressure levels in the near wall downstream of the sphere, leading to a decrease in the pressure differential between the front and the rear of the sphere.

As Reynolds number increases further, the turbulent structures in the mixing layer become finer. The separated shear layer loses momentum and thus separates earlier, resulting in an increase in drag coefficient (Bakic and Peric, 2005). In this super-critical Reynolds number region, the wake flow was found to be fully turbulent with an offset from the streamwise axis (Taneda, 1978).

Although in-depth research was carried out for the flow past a sphere in a single-phase flow (air or water), reported results for experiments including a free surface remain rare. The influence of the free surface on a submerged sphere

travelling at a speed equivalent to Reynolds number 5000 was studied both experimentally and numerically by Hassanzadeh et al.,(2012), Ozgoren et al., (2012) and Ozgoren et al., (2013). For small immersion depths, Hassanzadeh et al. (2012) showed that the recirculating region in the half-lower side of the wake region is larger compared to the half-upper side. Furthermore, a strong interaction between the fluctuated streamwise and transverse velocities in the half-lower side of the wake region was observed leading to a higher mixing flow rate. At an immersed depth to diameter ratio of 0.25 (from the top side of the sphere), a strong interference between the sphere wake and the free surface was noticed by Ozgoren et al. (2013). However, other literature of a sphere located at the free surface is non-existent, (Ozgoren et al. 2012).

Other bluff bodies located at the free surface such as cylinders have been studied. Yu et al. (2008) performed large-eddy simulations of the flow past a surface-piercing cylinder. The free surface was found to inhibit the vortex generation in the near wake. At Fr ~ 0.8, the flow exhibits 2-D vortex structures in the deep wake, whereas nearer to the free-surface 3-D vortex structures are observed. The intensity of the vortices shed decreases further as Froude number increases. At a higher Reynolds number ~ $1.0x10^5$, the free-surface effects on the vortex structures in the near wake become less significant and the wake features a flow similar to a 2-D flow without a free surface. The flow past bluff bodies located at the free surface is therefore strongly related to both Reynolds number and Froude number.

The aim of the work presented is to carry out a systematic experimental investigation of the influence of speed on the observed flow using a towing tank, for a 225mm diameter sphere with 50% immersion, and thereby classify the flow regimes and how the total drag varies alongside these flow changes. A preliminary numerical analysis of these flows is reported in James et al (2013).

2 Experimental set-up

The flow past a sphere located at the free surface, was studied over the critical Reynolds number range, $2.0x10^5 \leq Re \leq 4.4x10^5$, and the Froude number range, $0.7 \leq Fr \leq 1.5$. Experiments were carried out in the 30 m long, 2.4 m wide and 1.2m deep Lamont tank at the University of Southampton.

2.1 Model

A sphere was constructed based on a youth-size basketball covered with glass-fibre and epoxy resin. The resulting sphere diameter, D, is 225 mm. The sphere weighs 1.38 kg and was ballasted with 1.7 litres of fresh water in order to obtain neutral buoyancy. A vent was specifically placed at the rear of the sphere for this purpose. A 5% margin was allocated in the neutral buoyancy calculation to ensure that only limited force would be acting upwards, protecting the mounting system on the carriage. As shown in Figure 1, a 16-mm-diameter pipe is fixed at the rear of the sphere and secured in the resin. Hoerner (1935) indicates that with a rear spindle diameter less than D/4, the flow should not be significantly altered. The attachment pipe goes back up vertically at a distance D/2 from the rear of the sphere. The mid plane of the sphere is located at the static free surface, the vertical pipe should have very little influence on the flow regime of the sphere. Figure 2 shows the final experimental set-up.

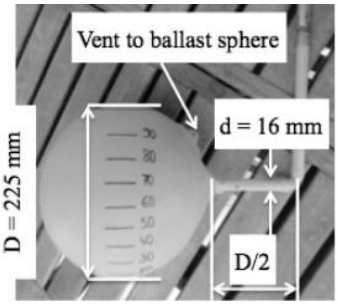

Fig.1 Sphere model with rear spindle attachment

2.2 Data acquisition

The sphere mounting system was attached onto a dynamometer recording both drag and side forces, using a sampling frequency of 100 Hz. This dynamometer is based on the electrical force transducer principle. A Linear Varying Displacement Transformer (LVDT) is positioned onto a flexure, which can move in one direction only. Providing that a calibration procedure is applied before testing, the force applied onto the sphere during a run can be obtained. A calibration process consists in applying several known weights and recording the corresponding amplified output voltages. A linear curve is fitted though the data points in order to get the rate to apply to the electrical response. Figure 3 shows the resultant calibration response undertaken with weights ranging from 2.5 N up to 10 N, with an increment of 2.5 N. An above-water camera was placed on the carriage in order to observe the wave created by the sphere.

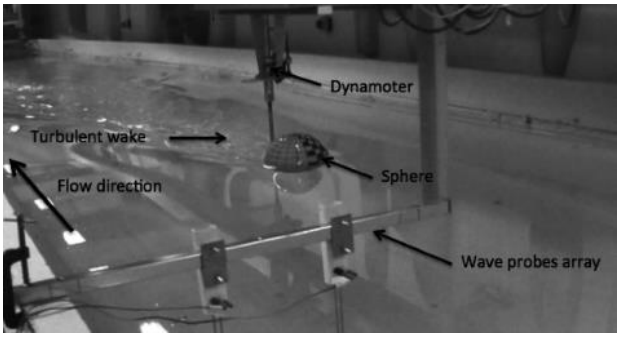

Fig.2 Overview of experiment set-up in the Lamont tank taken from side of tank. Direction of tow is from NW to SE.

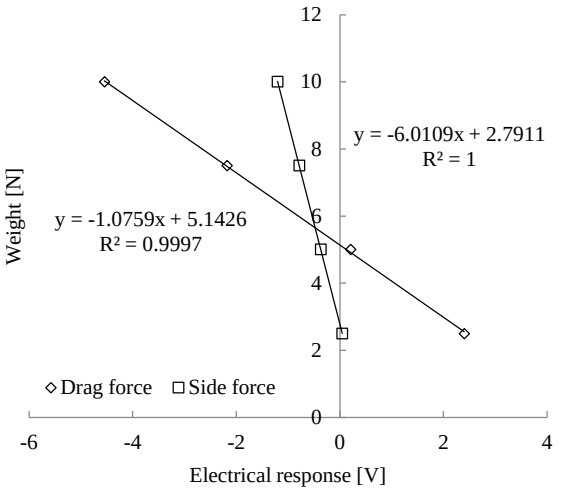

Fig.3 Calibration plot for drag and side forces with a least-square fit generating response slope.

2.2 Testing plan

The sphere was towed over speeds ranging from 1.0 $m.s^{-1}$ up to 2.2 $m.s^{-1}$, in incremental steps of 0.2 $m.s^{-1}$, and further data points were obtained around the transitional point. Three runs were performed at each speed to ensure reliability of the data. The equivalent depth-based Froude number for the tested speeds is between 0.3 and 0.7 (i.e. within the sub-critical flow range where depth effects are expected to be negligible (Molland et al., 2011)).

The tank water temperature was recorded with a calibrated digital thermometer as 6° Celsius. All results presented in this paper are corrected to a reference temperature of 15°C for towing tank testing using the IITC method (ITTC, 2014). In defining Reynolds number and other non-dimensional quantities, the density of fresh water for 15°C is taken as 999.1 $kg.m^{-3}$ and kinematic viscosity is 1.14 $x10^{-6}$ $m^2.s^{-1}$ (Newman, 1977).

3 Results

3.1 Qualitative results

Figure 4(a) defines a horizontal angle θ_{xy} and 4(b) vertical angle θ_{xz} as recorded from the above-water camera positioned above the sphere. The regular grid marked on the sphere was used to evaluate these angles. Figure 5 shows the recorded variation of θ_{xy} and θ_{xz} as a function of Reynolds number. A matrix of these photographs is presented in Figure 6. From this figure, the spray angles from both top (plane x-y) and side (plane x-z) views were measured to study the variation with speed. The angle, θ_{xy}, is defined between the stagnation point at the front of the sphere ($\theta_{xy} = 0°$) and the point at which the flow separates around the sphere at the calm free surface plane. Throughout this paper, this point is referred to as separation point. The angle, θ_{xz}, considers the angle between the stagnation point ($\theta_{xz} = 0°$) and the top of the bow wave in a plane perpendicular to the calm free surface.

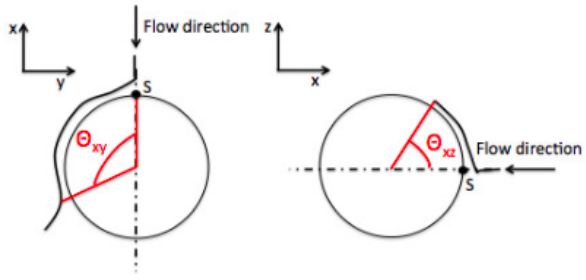

(a) From top view (b) From side view

Fig.4 Schematics of observed spray separation angles

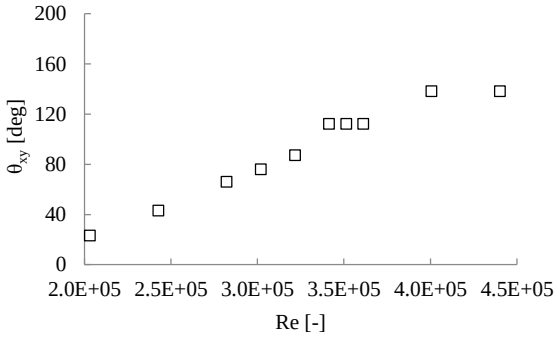

(a) Top view – Plane x-y

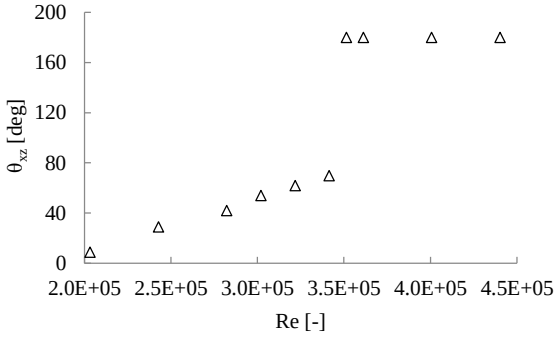

(b) Side view – Plane x-z

Fig.5 Spray angles obtained from the above-water photographs

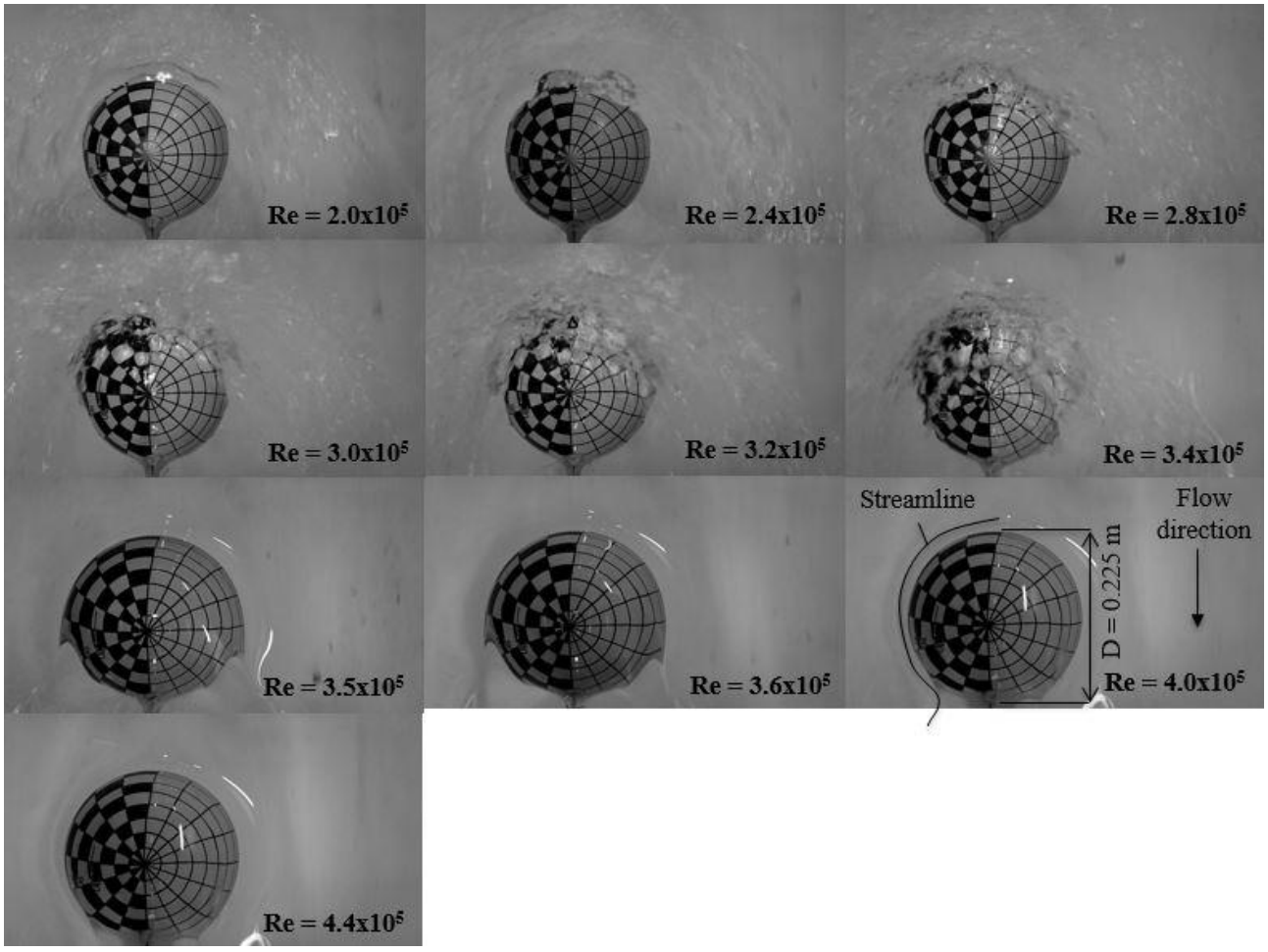

Fig.6 Test 1 – Matrix of photographs taken from an above-water camera, emphasizing the flow regime transition occurring around Re = 3.5 x10^5

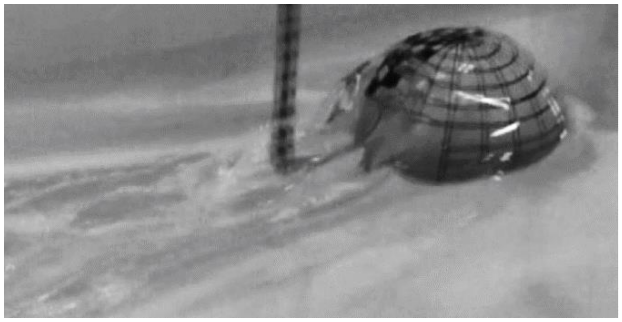

Fig.7 Turbulent wake behind the sphere at Re = 4.4x10^5

3.2 Quantitative results

The drag force is averaged over the steady portion of the drag force trace and is non-dimensionalised with respect to the sphere's projected area (Equation (1)) in order to allow comparison with previously tested spheres in air.

$$C_D = \frac{D}{0.5\rho A_p U^2} \qquad (1)$$

Where: D, is the sphere diameter; ρ, is the density of fresh water at 15°C; U is the measured steady run speed; and $A_p = \pi D^2/4$ is the full projected area.

The drag coefficient is plotted against Reynolds number for each data point in Figure 8. With three sets of data, the repeatability proved to be good with an averaged error of +/- 1% and a maximum error of 2%.

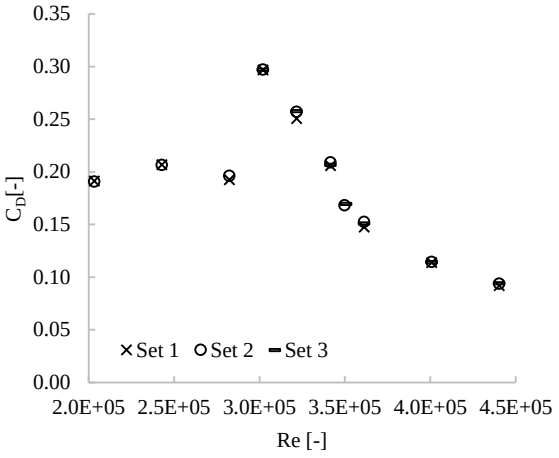

Fig.8 Drag coefficient, C_D, versus Reynolds number, Re, emphasising the drag crisis

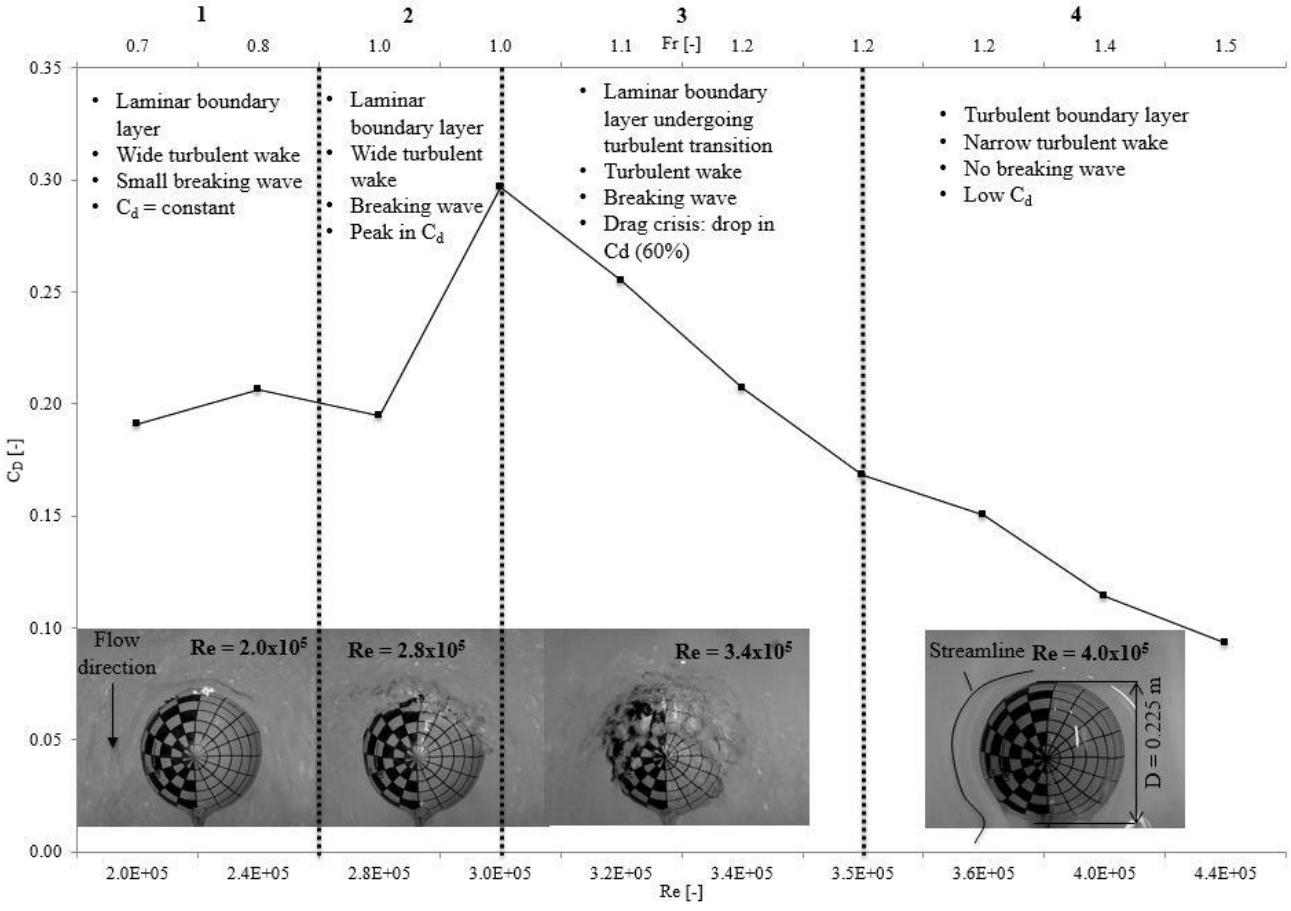

Fig.9 Flow regime taxonomy including with the mean drag curve versus Reynolds number ($Re = \frac{UD}{\nu}$) and Froude number ($Fr = \frac{U}{\sqrt{Dg}}$), and above-water photographs of key flow regime changes

4 Flow regime taxonomy and discussion

From the drag curve and the above-water photographs, a flow regime taxonomy is established in Figure 9. Four different flow regimes have been identified across the Reynolds number range $2.0x10^5 \leq Re \leq 4.5x10^5$.

Flow regime 1 – At the lower speeds, $Re \leq 2.5\ x10^5$ and $Fr \leq 0.9$, the drag coefficient has a fairly constant value of 0.2 and a small bow wave starts to form with an early laminar separation of the flow at the free surface plane ($\theta_{xy} \sim 40^o$), leading to a wide turbulent wake.

Flow regime 2 – As speed increases, the bow wave progressively gets larger. Moreover, the separation angle increases to $\theta_{xy} \sim 75^o$ as more momentum is carried through the laminar boundary layer and the flow rises up the sphere. In a single-phase flow, this increase in separation point would translate in a drag reduction. However the energy lost through the large breaking bow wave with a spray angle of $\theta_{xz} \sim 55^o$, appears to be much greater than the laminar boundary layer changes, since the drag coefficient increases by 50% to 0.3. This peak in drag rises rapidly at $Re = 3.0x10^5$ and $Fr = 1.0$.

Flow regime 3 – As the speed increases further, $3.0x10^5 \leq Re \leq 3.4x10^5$ and $1.0 \leq Fr \leq 1.2$, the horizontal plane separation angle increases to reach $\theta_{xy} \sim 110^o$. Although the bow wave also increases in size, the flow in the immersed portion of the sphere is presumed to have transitioned from laminar to turbulent that causes the drag to decrease sharply. This decrease in drag is well known under the term 'drag crisis' in single-phase flows.

Flow regime 4 – Suddenly at $Re = 3.5x10^5$ and $Fr = 1.2$, the bow wave stops breaking (oscillating in a manner similar to a classic hydraulic jump) towards the top of the sphere, around $\theta_{xz} \sim 70^o$ and it transforms into a smooth running sheet of fluid. From Bernoulli equation, this transition would in theory be expected to happen at $Fr = 1.0$, but it was delayed to $Fr = 1.2$ due to viscous and/or wave breaking effects. From a rear photograph taken at $Re = 4.4x10^5$ (Figure 7), it may be seen that the sheet of water is separating into two jet waves oscillating from one side to another. The sphere wetted surface area is maximal, and as speed increases the flow stays attached to the sphere for longer reducing further the pressure differential between the front and the rear of the sphere and hence decreasing the pressure drag.

6 Conclusions

In this paper, an initial taxonomy of the transitional flow past a sphere located at the air-water interface was established. Four key regimes are identified based on the measurements of the sphere drag, the horizontal flow separation angle and a vertical angle which measures the wetted extent of the flow over the top of the sphere.

Flow regime 1 – $2.5x10^5 \leq Re$ and $Fr \leq 0.9$

Laminar boundary layer with a wide turbulent wake and a small breaking bow wave, constant drag coefficient $C_D \sim 0.2$.

Flow regime 2 – $2.5x10^5 \leq Re \leq 3.0x10^5$ and $0.9 \leq Fr \leq 1.0$

Laminar boundary layer with a wide turbulent wake and a growing breaking wave, peak in drag coefficient, $C_D \sim 0.3$.

Flow regime 3 – $3.0x10^5 \leq Re \leq 3.4x10^5$ and $1.0 \leq Fr \leq 1.2$

Laminar boundary layer undergoing turbulent transition with a narrower turbulent wake and a large breaking wave, sharp decrease in drag coefficient, 'drag crisis'.

Flow regime 4 – $Re \geq 3.5x10^5$ and $Fr \geq 1.2$

Turbulent boundary layer with narrow turbulent wake. Absence of breaking wave, thin sheet of water running smooth on top of sphere, further decrease in drag coefficient but at a slow rate.

These tests were carried out for a single combination of diameter based Reynolds number and Froude number. Further work is on-going to establish how varying these combinations alters the transitions between the four flow regimes.

Acknowledgement

This work is part of an on-going PhD. I would like to thank my PhD sponsors: the University of Southampton and EPSRC. In particular, I would like to express my gratitude to all the people who helped me putting these experiments together: my father for helping me build the sphere model, my supervisors and the Wolfson Unit for their tank testing advice, and postgraduates of the Fluid-Structure Interaction group for helping during the towing tank tests.

References

Achenbach, E. (1972), 'Experiments on the flow past spheres at very high Reynolds numbers', Journal of Fluid Mechanics 54(03), 565.

Achenbach, E. (1974a), 'The effects of surface roughness and tunnel blockage on the flow past spheres', Journal of Fluid Mechanics 65(01), 113–125.

Achenbach, E. (1974b), 'Vortex shedding from spheres', Journal of Fluid Mechanics 62(02), 209–221. URL:http://www.journals.cambridge.org/abstractS0022112074000644

Bakic, V. and Peric, M. (2005), 'Visualisation of flow around sphere for Reynolds numbers between 22000 and 400000', Thermophysics ad Aeromechanics 12(3), 307–315.

Bakic, V., Schmid, M. and Stankovi, B. (2006), 'Experimental investigations of turbulent structures', pp. 97–112.

Hassanzadeh, R., Sahin, B. and Ozgoren, M. (2012), 'Large eddy simulation of free surface effects on the wake structures downstream of a spherical body', Ocean Engineering 54, 213–222.

Hoerner, S. F. (1965), Fluid Dynamic Drag, Hoerner Fluid Dynamics.

ITTC (2014), `ITTC recommended guidelines'.
URL: www.ittc.info

James, M. C., Turnock S. R., Hudson D. A. (2013), Flow past a sphere at the free-surface using URANS, 16th Numerical Towing Tank Symposium, Duisburg, Germany

Kim, K. J. and Durbin, P. A. (1988), 'Observation of the frequencies in a sphere wake and drag increase by acoustic excitation', Phys. Fluids 31(11), 3260–3265.

Kiya, M., Mochizuki, O. and Ishikawa, H. (2000), Challenging issues in separated and complex turbulent flows, in '10th International Symposium on Applications of Laser Techniques to Fluid Mechanics', Lisbon, Portugal, pp. 1–13.

Molland, A.F., Turnock, S. R. and Hudson, D.A. (2011), *Ship resistance and propulsion: practical estimation of ship propulsive power*, Cambridge, Cambridge University Press

Newman, J. N. (1977), Marine Hydrodynamics, The Massachussets Institute of Technology.

Ozgoren, M., Dogan, S., Okbaz, A., Sahin, B. and Akilli, H. (2012), 'Passive control of flow structure interaction between a sphere and free-surface', EPJ 25.

Ozgoren, M., Okbaz, A., Kahraman, A., Hassanzadeh, R., Sahin, B., Akilli, H. and Dogan, S. (2011), Experimental investigation of the flow structure around a sphere and its control with jet flow via PIV, in '6th IATS', number 5, pp. 16–18.

Sakamoto, H. and Haniu, H. (1990), 'A Study on Vortex Shedding From Spheres in a Uniform Flow', ASME 112(December), 386–392.

Taneda, S. (1956), 'Experimental investigation of the wake behind a sphere at low Reynolds numbers', Journal of the Physical Society of Japan 11(10), 1104 – 1108.

Taneda, S. (1978), 'Visual observations of the flow past a sphere at Reynolds numbers between 10^4 and 10^6', Journal of Fluid Mechanics 85(1), 187–192.

Yu, G., Avital, E. J. and Williams, J. J. R. (2008), 'Large Eddy Simulation of Flow Past Free Surface Piercing Circular Cylinders', Journal of Fluids Engineering 130(10), 101304.